Available online at www.sciencedirect.com
ScienceDirect
Trans. Nonferrous Met. Soc. China 32(2022) 3312−3320
Transactions of Nonferrous Metals Society of China
www.tnmsc.cn

Thermal reliabilities of Sn−0.5Ag−0.7Cu−0.1Al_2O_3/Cu solder joint

Jie WU[1*], Guo-qiang HUANG[2*], Song-bai XUE[3], Peng XUE[4], Yong XU[1]

1. College of Integrated Circuit Science and Engineering,
Nanjing University of Posts and Telecommunications, Nanjing 210003, China;
2. Sino-French Institute of Nuclear Engineering and Technology, Sun Yat-Sen University, Zhuhai 519082, China;
3. College of Materials Science and Technology,
Nanjing University of Aeronautics and Astronautics, Nanjing 210016, China;
4. School of Materials Science and Engineering, Nanjing University of Science & Technology, Nanjing 210016, China

Received 13 July 2021; accepted 7 January 2022

Abstract: The effects of trace addition of Al_2O_3 nanoparticles (NPs) on thermal reliabilities of Sn−0.5Ag−0.7Cu/Cu solder joints were investigated. Experimental results showed that trace addition of Al_2O_3 NPs could increase the isotheraml aging (IA) and thermal cyclic (TC) lifetimes of Sn−0.5Ag−0.7Cu/Cu joint from 662 to 787 h, and from 1597 to 1824 cycles, respectively. Also, trace addition of Al_2O_3 NPs could slow down the shear force reduction of solder joint during thermal services, which was attributed to the pinning effect of Al_2O_3 NPs on hindering the growth of grains and interfacial intermetallic compounds (IMCs). Theoretically, the growth coefficients of interfacial IMCs in IA process were calculated to be decreased from 1.61×10^{-10} to 0.79×10^{-10} cm^2/h in IA process, and from 0.92×10^{-10} to 0.53×10^{-10} cm^2/h in TC process. This indicated that trace addition of Al_2O_3 NPs can improve both IA and TC reliabilities of Sn−0.5Ag− 0.7Cu/Cu joint, and a little more obvious in IA reliability.

Key words: Sn−0.5Ag−0.7Cu solder; Al_2O_3 nanoparticles; isothermal aging; thermal cycling; thermal reliability

1 Introduction

With the development of 5G communication technology, the solder joint size was continuously decreased to echo the requirement of smaller and lightweight packaging [1,2]. However, smaller solder joint means higher current density and therefore more heat generation than before [3]. In addition, frequent on-off operation and long-term working of electronic devices often bring the internal solder joints into a thermal change environment, leading to an accumulation of stress and strain in the joint region due to different coefficients of thermal expansion of joint forming materials. Hence, thermal reliabilities of solder joints, including isothermal aging (IA) and thermal cyclic (TC) reliabilities will be greatly threatened [4]. It is well established that the thermal reliabilities of solder joints are strongly dependent on their microstructures, including the interface and its adjacent solder matrix [5,6]. In general, solder matrix with a refined microstructure, teamed with a thin and flat interfacial intermetallic compound (IMC) layer is often beneficial to microstructural stability, and thus enhancing thermal reliability.

Tailoring methods, such as solder modification and barrier metallic film deposition are taken, the former of which is more effective [7,8]. For solder modification, various alloys, intermetallics, micro- or nano-level oxides were selected to be added into original solder, especially for cost effective low-Ag

* Jie WU and Guo-qiang HUANG contributed equally to this work

Corresponding author: Song-bai XUE, E-mail: xuesb@nuaa.edu.cn; Yong XU, E-mail: xuyong@njupt.edu.cn

DOI: 10.1016/S1003-6326(22)66022-9

solders [9−11]. Among them, insoluble nano-oxides can remarkably enhance the joint reliability since the high stability characteristic of nano-oxides enables them to consistently hinder the motions of crystal defects and grain boundaries during IA or TC [11,12]. For instance, WEN et al [13] prepared Sn−1.0Ag−0.5Cu−0.05TiO_2 quaternary composite solder via vacuum alloy melting method. In TC reliability test, the shear strength of the joint doped with 0.05 wt.% TiO_2 NPs showed a slower decline of shear strength due to the inhibition effect on interfacial IMCs growth. Also, the ball shear strength of 1.0 wt.% TiO_2 NPs-doped Sn−0.7Cu solder joint maintained a relatively high level even after 8 cycles' reflow [14]. TSAO et al [15] electroplated α-Fe_2O_3 NPs-doped Sn solder on Cu substrate to fabricate a solder joint. The TC reliability result showed that as the nominal doping content of Fe_2O_3 NPs reached 0.032 g/L, the decrease rate of shear strength reached the maximum, due to the inhibited growth of interfacial IMC layer. These foreign nano-oxides maintained a relative dimensional stability during thermal service, continuously hindering the motions of crystal defects and grain boundaries, and finally decreasing the thermal fatigue ratio.

As economic and highly available nano-oxides, the valuable effects of α-Al_2O_3 NPs on the enhancement in properties of solder joint have been extensively reported [16,17]. However, few studies on the thermal reliabilities of Al_2O_3 NPs-doped solder joint were conducted. In this study, the cost effective Sn−0.5Ag−0.7Cu (SAC0507) low-Ag solder was selected as the target to enhance its IA and TC reliabilities, as evaluated with Weibull analysis. Multi-scale microstructure examinations were performed on the developed solder joints to deeply understand the microstructural factors of reliability improvement. The results of the work will promote the marketization of low-cost, high-reliability Sn−0.5Ag−0.7Cu solder and enrich the theory of modified solders with insoluble nano-material.

2 Experimental

In order to prepare SAC0507−(nano)Al_2O_3 solder paste, trace amount of Al_2O_3 NPs (0.1 wt.%, ~50 nm, Fig. 1) were weighed and then dispersed in ethanol and soldering flux sequentially. Afterwards, low-temperature ball milling machine (QM−DY4) was adopted to mechanically blend SAC0507 solder paste with Al_2O_3 NPs. Finally, organic solvents like PEG-600 and water-soluble flux, were added to ensure a suitable viscosity of composite paste.

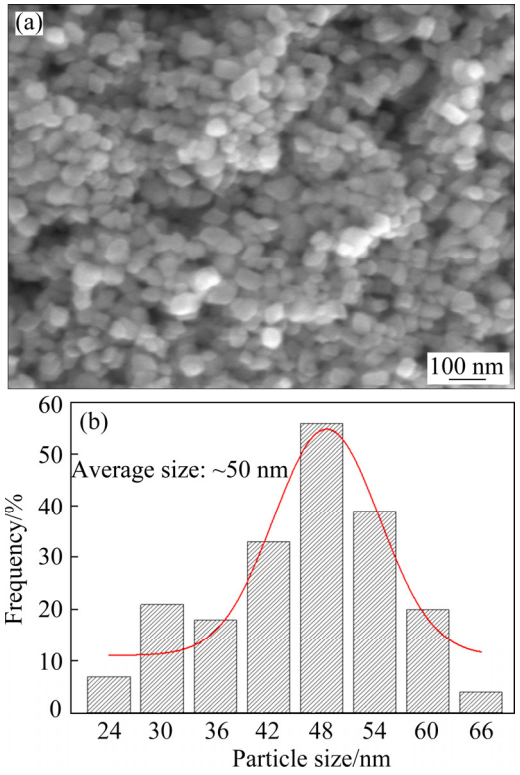

Fig. 1 Morphology of Al_2O_3 NPs (a) and particle size distribution (b)

In order to measure the shear force of solder joints during thermal services, several joint samples were made with reflow oven (Puhui, T−973M). For IA, the service temperature was adjusted to be 125 °C. For TC, the maximum and the minimum temperatures were set to be 125 and −45 °C, respectively, and the holding time was 20 min. STR−1000 Micro-joint strength tester (Rhesca, Japan) was used to measure shear forces of solder joints. The shear speed and tool stand-off were set to be 10 mm/min and 20 μm, respectively. In addition, fracture morphologies of solder joints were also observed with scanning electron microscopy (SEM, Hitachi S−3000N) to judge failure locations and analyze the underlying failure reason. Weibull analysis was used to calculate characteristic lifetimes of solder joint in different thermal services. Each group had 50 samples to obtain enough test data for Weibull distribution

analysis. The cycle or time when solder joint had a 63.3% drop in shear force was considered as the failure criterion.

In order to understand the enhanced mechanisms of joint reliability, interfacial samples were prepared via soldering SAC0507 and SAC0507−(nano)Al_2O_3 onto Cu substrate. Afterwards, a backscattered electron (BSE) detector-owned SEM (Hitachi S−3000N), and transmission electron microscope (TEM, LIBRA 200 FE) were assisted to observe the interfacial morphology.

3 Results and discussion

3.1 Weibull distribution and characteristic life

The characteristic lifetimes of SAC0507/Cu and SAC0507−(nano)Al_2O_3/Cu solder joints in IA and TC services were calculated with Weibull distribution analysis. Out of 50 samples for each group, the failure numbers of SAC0507/Cu and SAC0507−(nano)Al_2O_3/Cu in IA were 29 and 23, respectively, and those in TC were 24 and 19, respectively. In order to better fit the experimental data, a three-parameter Weibull cumulative distribution function was used as a model [18]:

$$F(t)=0 \quad \text{for} \quad t<t_0 \tag{1}$$

$$F(t)=1-\exp[-(t-t_0)/(\eta-t_0)^{\beta}] \quad \text{for} \quad t>t_0 \tag{2}$$

where t is failure time or cycle, t_0 is failure free time or cycle, before which no failure occurs, η is the characteristic lifetime to 63.3% failure, β is the shape parameter with original time shifted to t_0. Here, t_0 values of SAC0507/Cu and SAC0507−(nano)Al_2O_3/Cu solder joints in IA were 600 and 680 h, respectively, and those in TC were 1450 and 1700 cycles, respectively.

The cumulative density function $F(t)$ should be estimated to calculate the characteristic lifetime. A median ranking approach was used to describe $F(t)$ [19]:

$$F(t)=(i-0.3)/(n+0.4) \tag{3}$$

where i is the failure sample order, and n is the failure number.

Figure 2 provided the actual failure time, cycle, and the corresponding $F(t)$. Based on the data and Eq. (2), least-square analysis can be obtained as follows:

$$\ln[-\ln(1-F(t))]=\ln(t-t_0)-\beta\ln(\eta-t_0) \tag{4}$$

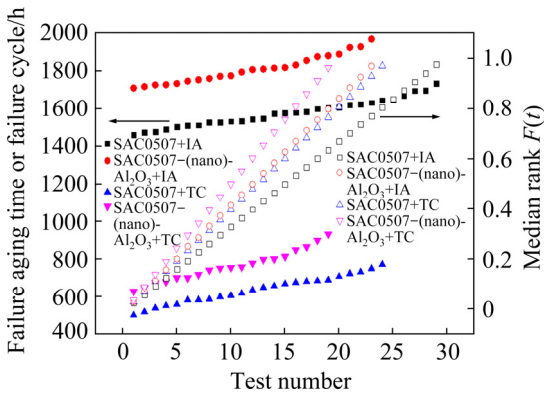

Fig. 2 Data statistics of failure samples

Figure 3 showed the final plotted results of the relationship between $\ln[-\ln(1-F(t))]$ and $\ln(t-t_0)$. These discrete points were linearly fitted, and the final IA reliability formula of SAC0507/Cu and SAC0507−(nano)Al_2O_3/Cu solder joints were expressed in Eqs. (5) and (6), respectively:

$$\ln[-\ln(1-F(t))]=1.47\ln(t-260)-7.59 \tag{5}$$

$$\ln[-\ln(1-F(t))]=1.31\ln(t-390)-6.73 \tag{6}$$

The TC reliability formula of SAC0507/Cu and SAC0507−(nano)Al_2O_3/Cu solder joints were expressed in Eqs. (7) and (8), respectively:

$$\ln[-\ln(1-F(t))]=1.18\ln(t-750)-6.62 \tag{7}$$

$$\ln[-\ln(1-F(t))]=1.17\ln(t-1150)-5.79 \tag{8}$$

The shape parameter β can be obtained from the slope of linear fitted curve, and the characteristic lifetime η can be calculated from the intercept. It can be calculated that trace Al_2O_3 NPs addition increased the IA characteristic lifetime of Sn−0.5Ag−0.7Cu/Cu joint from 662 to 787 h, and

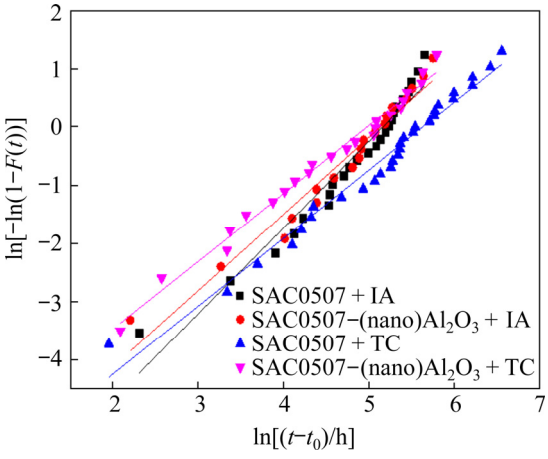

Fig. 3 Weibull plots with failure time or cycle

TC characteristic lifetime from 1597 to 1824 cycles. In addition, a slightly higher enhancement was observed in IA reliability (18.8%) than that in TC reliability (14.2%). This was related with stress impressed on the joint, distribution of Al_2O_3 NPs, and interfacial microstructure evolution during two different thermal environments.

3.2 Shear force and fracture morphology

Figure 4 shows the changes of shear forces under different thermal environments. It is clear that as IA time or TC cycle increased, the shear forces of all joints decreased, and a smaller decrease rate occurred in the Al_2O_3 NPs-doped joint samples. However, with further increase in aging time and thermal cycle, the drop rate of Al_2O_3 NPs-doped joint became larger than that of the original joint. It is probably due to the agglomeration of Al_2O_3 NPs that had the potential to initiate micro-cracks. After aging for 402 h, the shear forces of SAC0507/Cu and SAC0507−(nano)Al_2O_3/Cu solder joints dropped to 33 and 43.8 N, respectively, about 37.1% and 25.8% lower than the original. In addition, after subjected to 1200 TC cycles, shear forces of the above two kinds of joints decreased to 24.5 and 35.8 N, having a 52% and 37.5% drop, respectively. It was clear that trace addition of Al_2O_3 NPs slowed down the decrease of shear forces to some extent. Although the total IA time was equivalent to the accumulated holding time of TC at high temperature, the joint samples subjected to TC were more prone to fail due to cyclic stress and strain. The final increase in drop rate of shear forces of Al_2O_3 NPs-doped joint samples may be related to agglomeration of Al_2O_3 NPs.

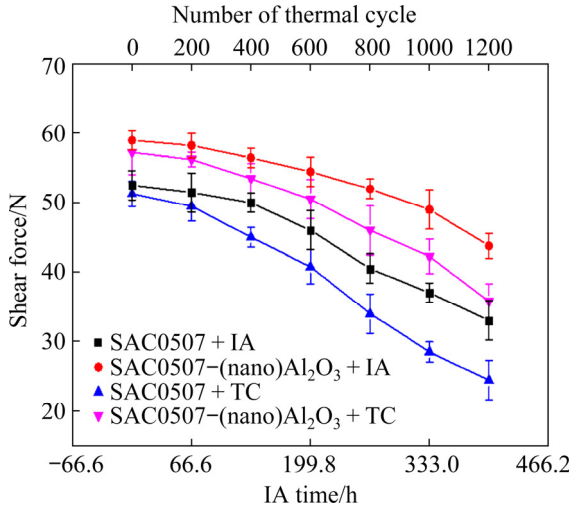

Fig. 4 Changes of joint shear forces during TC and IA

Generally, fracture morphology of one joint can reflect the corresponding fracture mode [20]. Figure 5 presents the fracture morphologies of SAC0507/Cu and SAC0507−(nano)Al_2O_3/Cu solder joints before and after being subjected to different thermal services. For as-reflowed SAC0507/Cu solder joint, its fracture displayed a typical ductile mode (Fig. 5(a)), which was the same with that of Al_2O_3 NPs-doped joint, as shown in Fig. 5(b). However, the dimples became more circular, indicating an enhancement in joint strength. When subjected to aging for 400 h, the dimples on the fracture of non-doped solder joint were further elongated and those of Al_2O_3 NPs-doped also became lager in diameter (Figs. 5(c) and (d)). But the average sizes of dimples of Al_2O_3 NPs-doped solder joint were still smaller than those of the non-doped solder joint. Moreover, coarsened Cu_6Sn_5 IMCs were found in the dimples of non-doped solder joint, whereas smaller Cu_6Sn_5 IMCs besides tiny Al_2O_3 agglomerations were found in the dimples of Al_2O_3 NPs-doped solder joint. This indicates that the addition of Al_2O_3 NPs can decrease the coarsening rate of IMCs in solder, which is conducive to slowing down the joint strength degradation. After 1200 TC cycles, the fracture surface of the non-doped joint became flatter. More obvious river patterns with a few cracks were observed on the fracture surface (Fig. 5(e)). The fracture location was identified to be Cu_6Sn_5 IMCs. This implies that the joint fractured at interfacial Cu_6Sn_5 IMCs with a brittle fracture mode. However, for Al_2O_3 NPs-doped joint, even after 1200 TC cycles, the fracture mode was still the microvoid accumulation ductile fracture (Fig. 5(f)). It can be concluded that doping Al_2O_3 NPs into solder can enhance the TC reliability of solder joint, which is a little bit more effective in IA reliability due to different forms of stress and strain impressed.

3.3 Evolution of interfacial microstructure

Figure 6 shows the interfacial microstructures of SAC0507/Cu and SAC0507−(nano)Al_2O_3/Cu solder joints before and after being subjected to IA and TC services. For the as-reflowed solder joints, the rod-like Cu_6Sn_5 IMCs were distributed in the solder matrix near the interface, which were refined into short rods after trace doping of Al_2O_3 NPs

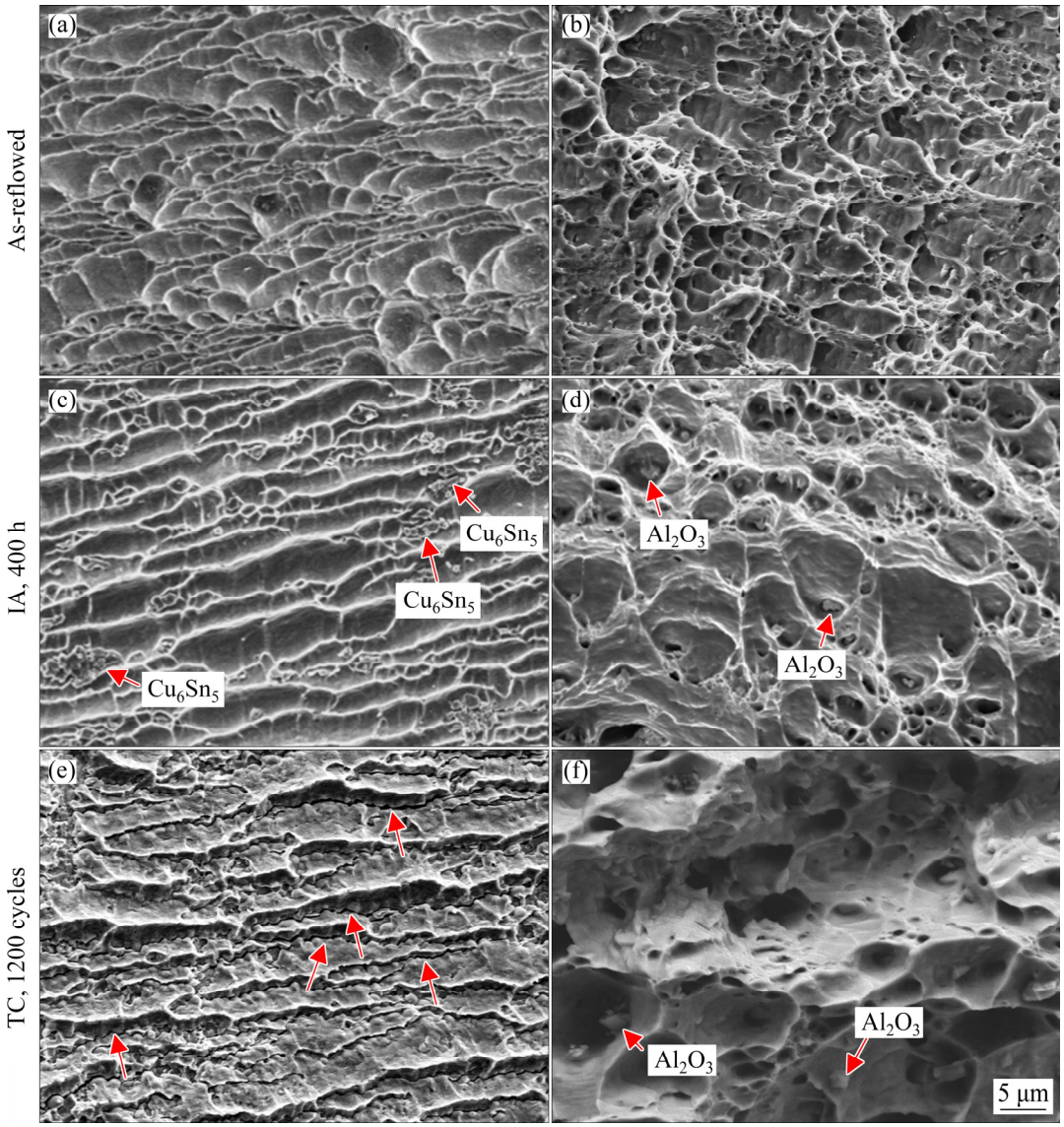

Fig. 5 Fracture morphologies of SAC0507/Cu (a, c, e) and SAC0507−(nano)Al_2O_3/Cu (b, d, f) solder joints

(Figs. 6(a) and (b)). Also, the morphology of the interfacial IMCs was changed from hill-like to layer-shaped. Few Ag_3Sn IMCs were observed due to low Ag content. After IA for 400 h, the Cu_6Sn_5 IMCs coarsened and the interfacial IMC layer thickened along with the formation of a new Cu_3Sn IMC layer for both solder joints, with a lower coarsening/thickening rate for nano-Al_2O_3-doped solder joint (Figs. 6(c) and (d)). It corresponded well to the decrease tread of shear forces. Specifically, Al_2O_3 agglomerations were found near the interface of IMCs, which may become a potential threat and induce micro-cracks. For solder joints subjected to TC (Figs. 6(e) and (f)), coarsening of Cu_6Sn_5 IMCs distributed in solder matrix and thickening of interfacial IMC layers also occurred. As expected, Al_2O_3 NPs-doped solder joint shows a low coarsening/thickening rate. Unlike IA solder joints, a few cracks were observed after 1200 TC cycles. Such a difference can be attributed to different forms of thermal stress in both cases. Figure 7 shows the detailed microstructure of solder matrix near the interface after IA and TC. It is clear that in both cases, Al_2O_3 NPs were still round in shape, with a size of 90−120 nm, and easily distributed at the grain boundaries. This suggests that despite the long time of thermal service, Al_2O_3 NPs can maintain their nano-size effect, pinning the movements of grain boundaries or dislocations and ultimately improving the thermal reliabilities of solder joint. The high dislocation density around the Al_2O_3 NPs justifies the role they play in dislocation hindrance.

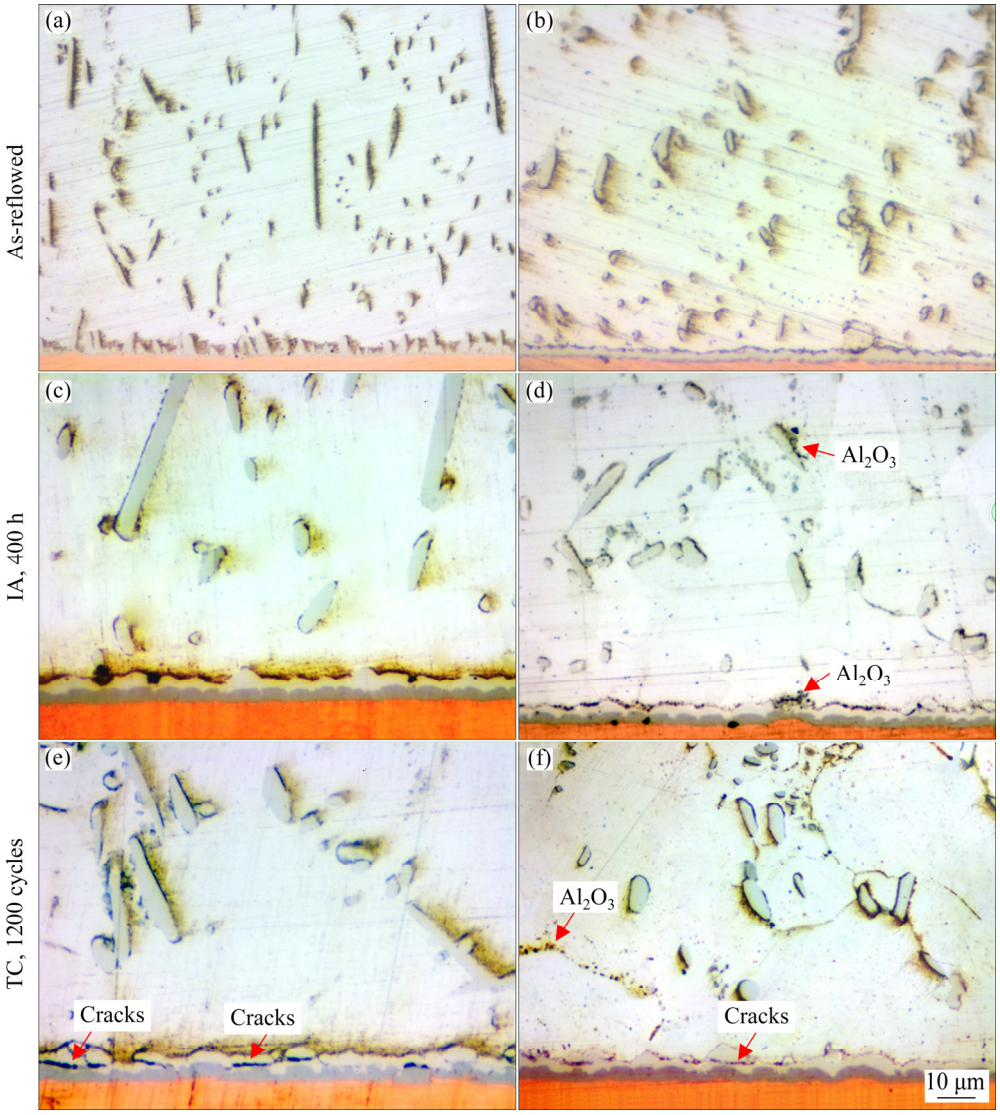

Fig. 6 Interfacial microstructures of SAC0507/Cu (a, c, e) and SAC0507−(nano)Al_2O_3/Cu (b, d, f) solder joints

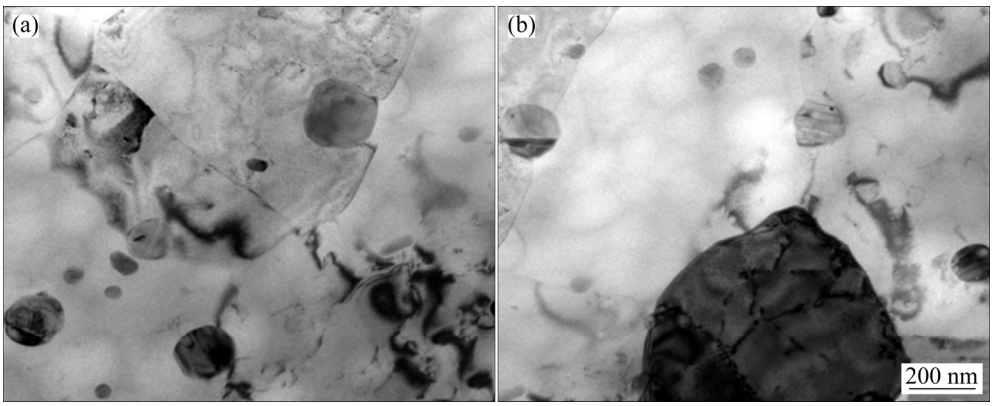

Fig. 7 TEM images of SAC0507−(nano)Al_2O_3/Cu solder matrix: (a) IA for 400 h; (b) TC for 1200 cycles

3.4 Evolution of interfacial IMC layer

Figure 8 shows the BSE micrographs of interfacial IMC layers at SAC0507/Cu and SAC0507−(nano)Al_2O_3/Cu interfaces. Prior to IA or TC service, scallop-shaped mixed with hill-like IMCs grew at SAC0507/Cu interface (Figs. 8(a) and (b)). With 0.1 wt.% Al_2O_3 NPs addition, the Cu_6Sn_5 grains coalesced into layer-like due to

hindering atom interdiffusion. When subjected to IA, the interfacial IMCs of both SAC0507/Cu and SAC0507−(nano)Al_2O_3/Cu solder joints had a further growth with the emergence of interfacial Cu_3Sn IMCs, and the morphology of interfacial IMC layer changed to layer-like morphology (Figs. 8(c) and (d)). It is clear that doping of 0.1 wt.% Al_2O_3 NPs could slow down the growth of interfacial IMC layer at the SAC0507/Cu interface, with the layer thickness measured to be 7.1 and 4.6 μm, respectively. For both solder joints subjected to 1200 TC cycles, the morphology of interfacial IMCs also became layer-like morphology (Figs. 8(e) and (f)), and the thickness of interfacial IMC layer increased to 8 and 4.9 μm, respectively. A few cracks emerged at the interfacial IMCs of non-doped solder joint.

Table 1 summarized the detailed thickness change during IA and TC processes. Here, the observation interval time (67 h) of the aging sample is approximately equivalent to the total high temperature holding time of 200 cycles in TC. Whether in IA or in TC process, the growth of interfacial IMC layer is a process of solid−solid diffusion, following the classic diffusion formula [21]:

$$x_t = x_0 + \sqrt{\bar{D}t} \tag{9}$$

where x_t is the thickness of interfacial IMC layer after IA and TC service for time t, x_0 is the initial thickness of interfacial IMC layer, and $\bar{D}$ is the average diffusion coefficient. According to Eq. (9), linear fitting was operated between the layer thickness of interfacial IMCs and the square root of aging time in IA and TC (Fig. 9). The slopes of linear fitted curves of SAC0507/Cu and SAC0507−(nano)Al_2O_3/Cu solder joints during IA are 0.127 and 0.089, respectively, and those during TC are 0.096 and 0.073, respectively. After calculation, the average diffusion coefficients of interfacial IMC layers at SAC0507/Cu and SAC0507−(nano)Al_2O_3/Cu interfaces during IA

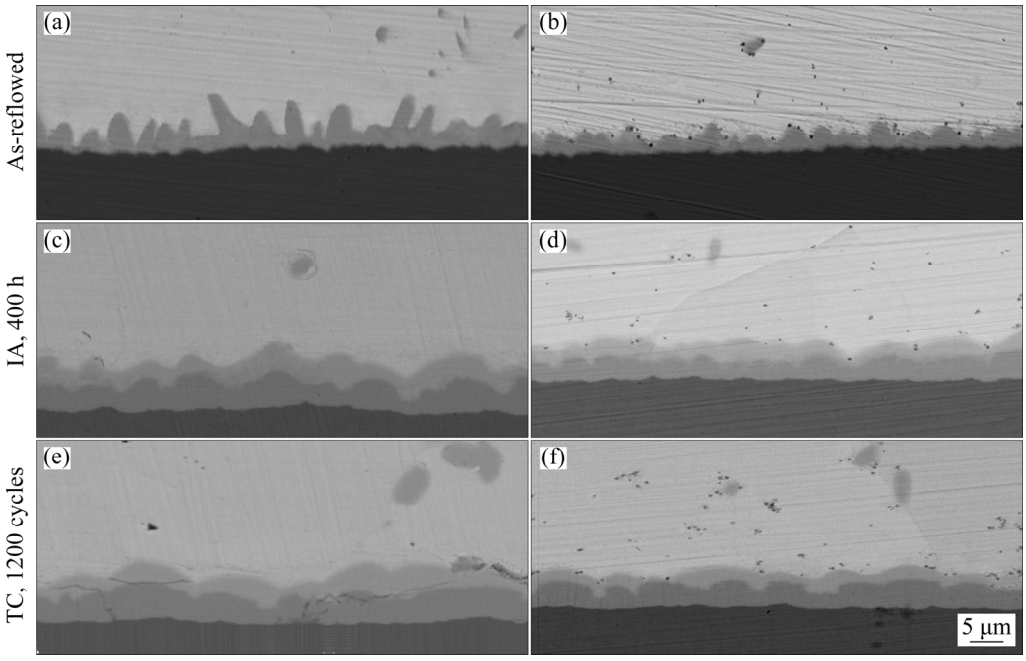

Fig. 8 BSE micrographs of interfacial IMCs of SAC0507/Cu (a, c, e) and SAC0507−(nano)Al_2O_3/Cu (b, d, f) solder joints

Table 1 Detailed thickness values during IA and TC

Solder alloy	Thickness of interfacial IMCs/μm											
	IA time/h						TC cycles					
	67	134	200	267	333	400	200	400	600	800	1000	1200
SAC0507	5.6	5.9	6.2	6.5	6.8	7.1	6.0	6.4	6.9	7.3	7.5	8.0
SAC0507−(nano)Al_2O_3	3.4	3.7	4.0	4.1	4.3	4.6	3.5	3.8	4.1	4.3	4.5	4.9

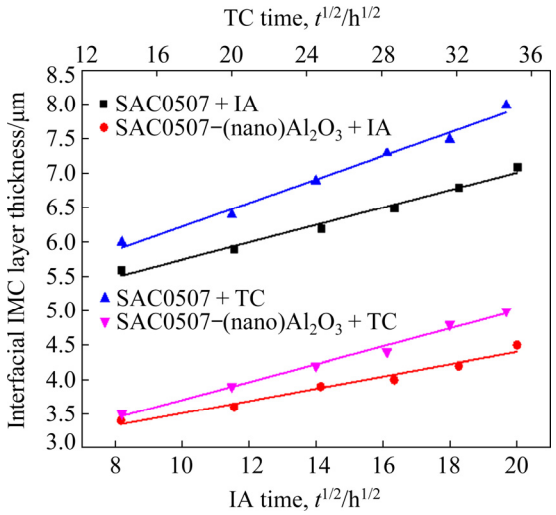

Fig. 9 Detailed thickness change of interfacial IMC layer during IA and TC

were 1.61×10^{-10} and 0.79×10^{-10} cm^2/h, and those during TC were 0.92×10^{-10} and 0.53×10^{-10} cm^2/h, respectively. Clearly, trace addition of Al_2O_3 NPs can effectively reduce the average diffusion coefficients of interfacial IMC layers. In addition, the decline rates in IA and TC were 50.9% and 42.6%, respectively. Also, it indicated a little bit more effective inhibition effect on interfacial IMCs growth during IA.

4 Conclusions

(1) Trace addition of Al_2O_3 NPs enhanced both IA and TC reliabilities of solder joints, especially the TC reliability. The calculated characteristic lifetimes of SAC0507/Cu and SAC0507−(nano)Al_2O_3/Cu solder joints during IA were 662 and 787 h, respectively, and those during TC were 1597 and 1824 cycles, respectively.

(2) During TC and IA services, the shear forces of solder joints decreased with increasing TC cycle and aging time, and Al_2O_3 NPs-doped solder joint had a slower decrease rate of shear force.

(3) Adding Al_2O_3 NPs helped SAC0507−(nano)Al_2O_3 maintain a higher ductility than the non-doped solder joint. The fracture of Al_2O_3 NPs-doped solder joint displayed a typical ductile fracture mode with smaller dimples, whereas an obvious brittle fracture occurred in the SAC0507/Cu solder joint in TC.

(4) During IA and TC service, the coarsening of matrix microstructure was slowed down in the Al_2O_3 NPs-doped solder joint. In addition, doping Al_2O_3 NPs effectively decreased the average growth coefficients of interfacial IMCs at SAC0507/Cu and SAC0507−(nano)Al_2O_3/Cu interfaces from 1.61×10^{-10} to 0.79×10^{-10} cm^2/h in IA, and from 0.92×10^{-10} to 0.53×10^{-10} cm^2/h in TC.

Acknowledgments

This work was financially supported by the National Natural Science Foundation of China (Nos. 52105369, 61974070), Natural Science Foundation of the Jiangsu Higher Education Institutions of China (No. 20KJB460008), Natural Science Foundation of Jiangsu Province, China (No. BK20200746), and NUPTSF (No. NY220077).

References

[1] WANG Y T, WATANABE A O, OGURA N, RAJ P M, TUMMALA R. Sintered nanocopper paste for high-performance 3D heterogeneous package integration [J]. Journal of Electronic Materials, 2020, 49(11): 6737−6745.

[2] LIN T H, KANNO K, WATANABE A O, RAJ P M, TUMMALA R R, SWAMINATHAN M, TENTZERIS M M. Broadband and miniaturized antenna-in-package (AiP) design for 5G applications [J]. IEEE Antennas and Wireless Propagation Letters, 2020, 19(11): 1963−1967.

[3] WANG P H, LEE Y C, LEE C K, CHANG H H, CHIANG K N. Solder joint reliability assessment and pad size studies of FO-WLP with glass substrate [J]. IEEE Transactions on Device and Materials Reliability, 2021, 21(1): 96−101.

[4] LI J H, ZHANG Y X, ZHANG H L, CHEN Z, ZHOU C, LIU X H, ZHU W H. The thermal cycling reliability of copper pillar solder bump in flip chip via thermal compression bonding [J]. Microelectronics Reliability, 2020, 104: 113543.

[5] LI Xue-mei, SUN Feng-lian, ZHANG Hao, XIN Tong. Effect of temperature on interface diffusion in micro solder joint under current stressing [J]. Transactions of Nonferrous Metals Society of China, 2015, 25: 1699−1703.

[6] KUO J C. Effects of bismuth additions on mechanical property and microstructure of SAC-Bi solder joint under current stressing [J]. Microelectronics Reliability, 2021, 117: 114041.

[7] WU M, QU X H, HE X B, QIN R L. Interfacial reactions between Sn−2.5Ag−2.0Ni solder and electroless Ni(P) deposited on SiC_p/Al composites [J]. Transactions of Nonferrous Metals Society of China, 2010, 20(6): 958−965.

[8] KELLY M B, MAITY T, NAZMUS SAKIB A R N, FREAR D R, CHAWLA N. Influence of substrate surface finish metallurgy on lead-free solder joint microstructure with implications for board-level reliability [J]. Journal of Electronic Materials, 2020, 49(5): 3251−3258.

[9] LEE C J, MIN K D, JEONG H, HWANG B U, JUNG S B. The fabrication of Ni-MWCNT composite solder and its

reliability under high relative humidity and temperature [J]. Journal of Electronic Materials, 2020, 49(11): 6746−6753.
[10] WANG Hao-zhong, HU Xiao-wu, JIANG Xiong-xin. Effects of Ni modified MWCNTs on the microstructural evolution and shear strength of Sn−3.0Ag−0.5Cu composite solder joints [J]. Materials Characterization, 2020, 163: 110287.
[11] HAN Yong-dian, YANG Jia-hang, XU Lian-yong, JING Hong-yang, ZHAO Lei. Effect of transient current bonding on interfacial reaction in Ag-coated graphene Sn−Ag−Cu composite solder joints [J]. Transactions of Nonferrous Metals Society of China, 2021, 31(8): 2454−2467.
[12] LIU Li-jun, ZHAO Xiu-chen, CHEN Ping, LIU Ying, WANG Yong, CHEN Wei-wei, WU Jia-qi. Effects of α-Fe_2O_3 additions on assembly reliability of electroplated Sn-based solder cap on Cu pillar bump during thermal cycling [J]. Journal of Electronic Materials, 2019, 48: 1079−1090.
[13] WEN Yan-ni, ZHAO Xiu-chen, CHEN Zhuo, GU Yue, WANG Yong, CHEN Zhi-wei, WANG Xin-yuan. Reliability enhancement of Sn−1.0Ag−0.5Cu nano-composite solders by adding multiple sizes of TiO_2 nanoparticles [J]. Journal of Alloys and Compounds, 2017, 696: 799−807.
[14] TANG Y, LI G Y, CHEN D Q, PAN Y C. Influence of TiO_2 nanoparticles on IMC growth in Sn−3.0Ag−0.5Cu−$x$$TiO_2$ solder joints during isothermal aging process [J]. Journal of Materials Science (Materials in Electronics), 2014, 25(2): 981−991.
[15] TSAO L C, WU M W, CHANG S Y. Effect of TiO_2 nanoparticles on the microstructure and bonding strengths of $Sn_{0.7}Cu$ composite solder BGA packages with immersion Sn surface finish [J]. Journal of Materials Science: Materials in Electronics, 2012, 23(3): 681−687.
[16] TIKALE S, PRABHU K N. Performance and reliability of Al_2O_3 nanoparticles doped multicomponent Sn−3.0Ag−0.5Cu−Ni−Ge solder alloy [J]. Microelectronics Reliability, 2020, 113: 113933.
[17] SHALABY R M, ELZANATY H. Effect of nano-Al_2O_3 particles on the microstructure and mechanical performance of melt-spun process Sn−3.5Ag composite solder [J]. Journal of Materials Science: Materials in Electronics, 2020, 31(8): 5907−5913.
[18] YEO C K, MHAISALKAR S, PANG H L J, YEO A. Experimental study of solder joint reliability in a 256 pin, 0.4 mm pitch PQFP [J]. Journal of Electronics Manufacturing, 1996, 6(2): 67−78.
[19] GONG He, YAO Yao, YANG Yu-ting. Size effect on the fracture of sintered porous nano-silver joints: Experiments and Weibull analysis [J]. Journal of Alloys and Compounds, 2021, 863(3): 158611.
[20] WU Ming, WANG Shan-lin, SUN Wen-jun, HONG Min, CHEN Yu-hua, KE Li-ming. Fracture pattern evolution of SnAgCu−SnPb mixed solder joints at cryogenic temperature [J]. Transactions of Nonferrous Metals Society of China, 2021, 31(9): 2762−2772.
[21] BAI Hai-long, LONG Zan, CHEN Jun-yu, GU Xing, LV Jin-mei, ZHAO Ling-yan, CHEN Dong-dong, YAN Ji-kang. Influence of Ag content on the formation and growth of intermetallic compounds in Sn−Ag−Cu solder [J]. Journal of Materials Science (Materials in Electronics), 2020, 31(13): 10105−10112.

Sn−0.5Ag−0.7Cu−0.1Al_2O_3/Cu 焊点的热可靠性

吴 洁[1]，黄国强[2]，薛松柏[3]，薛 鹏[4]，徐 勇[1]

1. 南京邮电大学 集成电路科学与工程学院，南京 210003；
2. 中山大学 中法核工程与技术学院，珠海 519082；
3. 南京航空航天大学 材料科学与技术学院，南京 210016；
4. 南京理工大学 材料科学与工程学院，南京 210016

摘 要：研究添加微量 Al_2O_3 纳米颗粒对 Sn−0.5Ag−0.7Cu/Cu 焊点热可靠性的影响。实验结果表明：添加微量 Al_2O_3 纳米颗粒可以将 Sn−0.5Ag−0.7Cu/Cu 接头的热时效特征寿命从 662 h 提高至 787 h，将接头的热循环特征寿命从 1597 次提高至 1824 次。此外，添加 Al_2O_3 纳米颗粒可以减缓热服役期间剪切力的降低，这得益于 Al_2O_3 纳米颗粒的钉扎效应可以阻碍晶粒和金属间化合(IMCs)物的生长。理论上，等温时效过程中界面 IMCs 的平均生长系数由 1.61×10^{-10} cm^2/h 降至 0.79×10^{-10} cm^2/h；热循环过程中界面 IMCs 的平均生长系数由 0.92×10^{-10} cm^2/h 降至 0.53×10^{-10} cm^2/h。这表明，添加微量 Al_2O_3 纳米颗粒可以提高 Sn−0.5Ag−0.7Cu/Cu 接头的热时效和热循环可靠性，且热时效可靠性的提升效果较为明显。

关键词：Sn−0.5Ag−0.7Cu 钎料；Al_2O_3 纳米颗粒；等温时效；热循环；热可靠性

(Edited by Wei-ping CHEN)